Mapping the "Forbidden" Transverse-Optical Phonon in Single Strained Silicon (100) Nanowire

Alvarado Tarun,[†,§] Norihiko Hayazawa,*[,†,§,⊥] Hidekazu Ishitobi,[†,§] Satoshi Kawata,[†,§,∥,⊥] Manfred Reiche,[‡] and Oussama Moutanabbir*[,†,‡,#]

[†]Nanophotonics Laboratory, RIKEN, The Institute of Physical and Chemical Research, 2-1 Hirosawa, Wako, Saitama 351-0198, Japan

[‡]Max Planck Institute of Microstructure Physics, Weinberg 2, Halle, 06120 Germany

[§]Near-field Nanophotonics Research Team, RIKEN, 2-1, Hirosawa, Wako, Saitama 351-0198, Japan

[#]Département de Génie Physique, École Polytechnique de Montréal, P.O. Box 6079, Station Centre-Ville, Montréal, Québec H3C 3A7, Canada

[∥]Department of Precision Science & Technology and Applied Physics, Osaka University, Suita, Osaka 565-0871, Japan

[⊥]CREST, Japan Science and Technology Agency, Kawaguchi, Saitama 332-0012, Japan

S *Supporting Information*

ABSTRACT: The accurate manipulation of strain in silicon nanowires can unveil new fundamental properties and enable novel or enhanced functionalities. To exploit these potentialities, it is essential to overcome major challenges at the fabrication and characterization levels. With this perspective, we have investigated the strain behavior in nanowires fabricated by patterning and etching of 15 nm thick tensile strained silicon (100) membranes. To this end, we have developed a method to excite the "forbidden" transverse-optical (TO) phonons in single tensile strained silicon nanowires using high-resolution polarized Raman spectroscopy. Detecting this phonon is critical for precise analysis of strain in nanoscale systems. The intensity of the measured Raman spectra is analyzed based on three-dimensional field distribution of radial, azimuthal, and linear polarizations focused by a high numerical aperture lens. The effects of sample geometry on the sensitivity of TO measurement are addressed. A significantly higher sensitivity is demonstrated for nanowires as compared to thin layers. In-plane and out-of-plane strain profiles in single nanowires are obtained through the simultaneous probe of local TO and longitudinal-optical (LO) phonons. New insights into strained nanowires mechanical properties are inferred from the measured strain profiles.

KEYWORDS: Nanowire, nanomembrane, strained silicon, nanoscale pattering, polarized micro-Raman spectroscopy, transverse-optical phonons
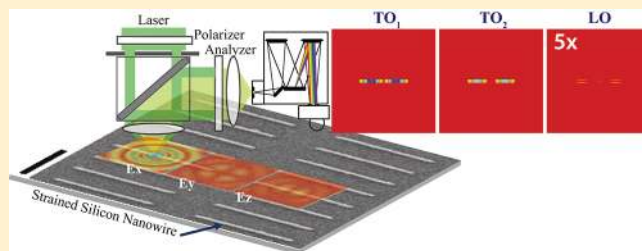
Strain and stress nanoengineering has emerged as a powerful strategy to expand the capabilities of Si-based nanoscale technologies.[1−11] This is attributed to the profound influence of strain on band structure and lattice symmetry of Si, which gives rise to advantageous electronic and optical properties. For instance, since the 65 nm technology node, the precise control of the amount and distribution of strain in Si devices has been used to ensure the continuity in performance enhancement and scaling of CMOS technology.[1,2] Moreover, strain engineering was demonstrated to alleviate design difficulties and performance degradation faced in the emerging nanowire-based architectures such as trigate and gate-all-around nanowire MOSFETs.[11] In addition to these applications in boosting the performance of Si transistors, the influence of strain in conjuncture with other quantum effects can also be exploited to design and engineer novel Si nanowire devices. In this perspective and based on the fact that the electronic structure of nano-materials can be tuned through quantum confinement or topological symmetries, recent theoretical studies suggested that strain can be employed to control the intrinsic properties of a single chemically homogeneous nanowire with the potential to induce charge separation without doping or creating an interface with other material.[8,9] These ab initio calculations demonstrate that local engineering of strain along the axis of a quantum-size Si nanowire can induce lowest unoccupied molecular orbitals and highest occupied molecular orbitals states to be localized in separate regions.[8,9] This effect results mainly from the crystal structure of the Si nanowire and quantum confinement effects strengthen the energy level offsets. Consequently, in a partially strained Si nanowire, the frontier energy levels of the strained part are simultaneously higher and lower than the unstrained part, effectively forming a type-II homojunction.
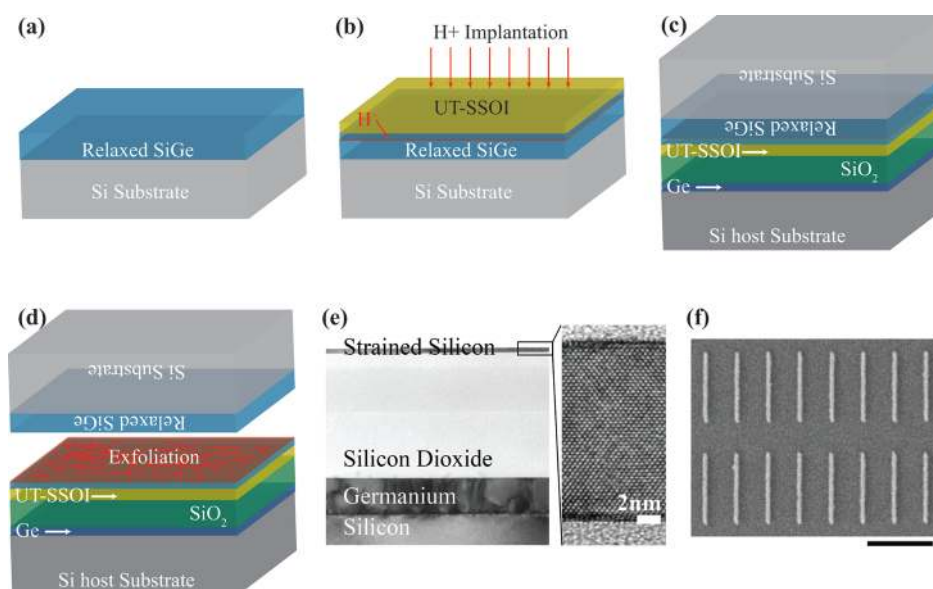
Figure 1. Schematic illustration of the process flow for the fabrication of background-free UT-SSOI using thin layer transfer. (a) Growth of relaxed $Si_{0.82}Ge_{0.18}$ relaxed buffer layer on Si(100) substrate; (b) growth of biaxially tensile strained Si on $Si_{0.82}Ge_{0.18}$ and subsequent hydrogen ion implantation into the grown heterostructure; (c) bonding of the hydrogen-implanted onto a host substrate on which Ge layer was grown followed by deposition of SiO_2 layer; (d) thermal annealing-induced layer exfoliation around the hydrogen implantation depth; (e) cross-section transmission electron microscopy image of the heterostructure obtained after the removal of the residual SiGe. Inset: high-resolution image of the 15 nm thin strained membrane and the corresponding diffraction pattern. (f) Scanning electron microscopy of the array of nanowires fabricated by electron beam lithography and reactive ion etching. The thickness, the width, and the length of the nanowires are 15 nm, 30 nm, and 1 μm, respectively.

The exploitation of the full potential of strain-engineered Si nanowire devices raises two major challenges. First, the precise control of strain during the fabrication process remains an outstanding task, which becomes even more difficult for quantum-size nanowires. Several processes have been proposed so far including the realization of germanium—silicon core—shell nanowires synthesized through metal-catalyzed vapor phase epitaxy.[3] This process is, however, associated with a number of undesired morphological instabilities.[12] The use of local stressors such as SiGe alloys and Si nitride lines can also be used to introduce strain, but this method can hardly be scaled as dimensions shrink.[13] The second challenge is related to development of accurate, less invasive, and sensitive techniques to probe on the nanoscale the strain and the associated changes in the nanowire properties. A number of techniques have been proposed to measure the amount and distribution of strain in Si nanoscale systems.[14−19] However, each of these techniques suffers a number of limitations such as being invasive or insensitive to all strain components, or having a limited spatial resolution. Tip-enhanced Raman spectroscopy is one of the promising techniques to investigate the strain distribution in the nanoscale,[15,20] however, the electric polarization condition around the tip-apex has not been well characterized as it strongly depends on the tip geometry and light illumination method.

In this work, we utilized ultrathin tensile strained silicon-on-insulator (UT-SSOI) membranes to fabricate strained Si nanowires using a top-down approach. The local strain and the involved free surface-induced strain redistribution during the formation of the nanowire are investigated using high-resolution polarized micro-Raman spectroscopy. We describe a method that permits the excitation of the "forbidden" transverse-optical (TO) phonons, which is critical for an accurate analysis of the strain in ultrathin strained Si nanowires. In-plane and out-of-plane strain profiles in single nanowires are obtained through this simultaneous probe of local longitudinal-optical (LO) and TO phonons. The profile of strain associated with TO Raman shifts across individual strained nanowires is analyzed and compared to LO related shifts. The intensity of the measured Raman spectra is analyzed based on three-dimensional field distribution of radial, azimuthal, and linear polarizations focused by a high numerical aperture (NA) lens. The effects of sample geometry on the sensitivity of TO measurement are considered. New insights into strained nanowires mechanical properties are also discussed based on the measured strain profiles.

Fabrication of Ultrathin Tensile Strained Si Nanowires. Figure 1a−d illustrates the process employed to fabricate UT-SSOI membranes. The 15 nm thick strained Si membranes were generated by the epitaxial growth of Si on ∼500 nm thick $Si_{1-x}Ge_x$ ($x \sim 0.18$) relaxed buffer layers deposited on Si(001) substrate. Using direct wafer bonding and ion-cut process,[21] the strained membrane was then transferred onto a handle substrate capped with ∼120 nm thick layer of Ge grown by molecular beam epitaxy. Prior to direct bonding, both substrates were covered by a plasma-enhanced chemical vapor deposited SiO_y layer. Figure 1e shows a cross-sectional transmission electron microscopy of the obtained structure with the Ge interlayer. Ordered arrays of strained Si nanowires were fabricated using these UT-SSOI membranes by combining electron beam lithography (JEOL JBX-6300) and reactive ion etching. The etching process was carried out at a temperature of −60 °C in a mixture of SF_6 (100 sccm) and O_2 (5 sccm) at a power of 40 W. The etching conditions were optimized to avoid damage at the newly formed nanowire edges. The investigated nanowires have a length of 1 μm and a diameter of 30 nm (Figure 1f). All the nanowires are aligned along the [110] direction and separated by

~500 nm from each other. The introduction of a highly absorptive Ge layer underneath the buried oxide was used to suppress the Si substrate background during Raman analysis[22] (see Figure S1 in Supporting Information). Using this material, only vibrational modes intrinsic to strained nanowires are detected. The Ge—Ge peak[23] centered at 301.0 cm^{-1} is far from interfering with the Si—Si peak of the strained membrane. This peak is insensitive to the stress in the SSOI and can be used as "wavenumber calibration" for Raman analysis as instabilities may occur during the experiment. For instance, slight changes in the light pass may result in a shift of the strained Si peak. These minute changes are caused by the polarizers, analyzers, and other optics associated with micro-Raman spectroscopy techniques and/or small changes in the focusing of the laser on the sample during scanning. These instabilities could make the strain analysis fraught with large uncertainties.

Methodology of TO Phonon Excitation in Strained Si Nanowire. Though imaging with only LO phonon is enough to obtain the in-plane strain distribution, Raman shifts from TO phonon are required for a more accurate characterization of strain. Indeed, the simultaneous probe of LO and TO phonons is of compelling importance to estimate both in-plane and out-of-plane strains. These quantities are critical to predict and control hole and electron relative mobility, which are related to vertical and lateral stress distributions.[24] In conventional backscattering geometry, the detection of Si(001) Raman scattering from TO phonon is generally forbidden. However, this is not the case when using high NA objective lens in terms of both excitation and detection of TO phonons. In an early report, Brunner et al.[25] have observed weak symmetry forbidden phonon modes in compressively strained Si film using polarized Raman spectroscopy under backscattering configuration with an objective lens having a NA of 0.95. Additionally, TO phonons can, in principle, be measured with off-axis[26,27] (oblique) polarized Raman spectroscopy or when the sample is not (001)-oriented.[28] Therefore, it is important to note the excitation of TO phonons in Si(001) cannot be restricted in micro-Raman spectroscopy analysis even under the backscattering configuration.[25,29,30] Indeed, TO phonon in strained Si(001) films under the backscattering configuration was recently excited and detected using linearly x-polarized light (parallel to the surface) focused with a high numerical aperture (NA) lens.[31,32] This is because the z-polarized component (longitudinal field) of focused light, which excites TO phonons, can be effectively generated using a high NA lens. However, y-polarized component, which is often ignored when using a linearly x-polarized excitation, is no longer negligible when a high NA lens is used due to depolarization effect. This depolarization effect at the diffraction-limited focus spot is considered in our analysis. The coexistence of LO phonon contribution in Raman signal due to y-polarized component, which cannot be suppressed by the analyzer during TO phonons measurement, reduces the accuracy of the technique. In this work, the effect of depolarization at focus generated by a high NA lens of different incident polarizations on the sensitivity and accuracy of TO phonons excitation is investigated. The relative intensities of TO and LO Raman modes have been taken into consideration to accurately interpret the Raman data of strained Si nanowires. Notwithstanding the numerous attempts to excite and detect TO phonons,[25−32] our work presents the first experimental investigation of TO-related strain behavior in individual nanostructures. It is also worth mentioning that the xy-polarized component (transverse field) of the focus light can

also excite TO phonons but the detection efficiency is generally too small since the radiation dipole is oriented normal to the surface. The electric field intensity distributions from a tightly focused lens is first calculated at different incident polarizations and then operated to the Si Raman tensor to estimate the Raman intensities of LO and TO optical phonons. Using a circular mask to block low NA components of the lens, radial, azimuthal, and linear polarizations are investigated.

Polarized micro-Raman measurement was carried out in backscattering configuration using a modified inverted optical microscope with a PZT driven xy stage[33] (see Figure S2 in Supporting Information). The polarization of the expanded incident beam, ~15×, from 532 nm laser was controlled via combination of a polarizer, half-waveplate and an 8-segmented radial-waveplate (Zpol: Nanophoton Inc.).[34] Focusing the radial and azimuthal light by a high NA lens generates a strong longitudinal (z-polarized) and pure transverse (xy-polarized) electric field, respectively. Radial or azimuthal light can be easily obtained by properly selecting the polarization of the incident light using the half-waveplate. Removing the radial-waveplate provides the linear polarization. The polarization-controlled incident light passed through a circular mask to reject the low NA component (NA < 1) and was then focused by a high NA (= 1.4), oil immersion lens. The mask is used to enhance the z-component. The backscattered Raman signal was collected by the same objective lens and delivered to an analyzer before being recorded by a spectrometer equipped with a liquid nitrogen-cooled charged couple device camera (CCD). The experimentally obtained wavelength repeatability and accuracy using Lorentzian fitting is ~0.02 cm^{-1}. This was obtained by calculating the standard deviation from 10 Raman measurements. The system spectral resolution (grating = 1800 g/mm, focal length = 640 mm, slit width = 100 μm) is ~0.02 nm. The accuracy and sensitivity of our Raman analysis were confirmed using high-resolution transmission electron microscoy-based methods. Collection of Raman signal uses the full NA of the lens. For the linear polarization experiment, the incident light was x-polarized parallel to the length of the nanowire, which is in the [110] direction (See Figure S2 in Supporting Information), and the scattered light was analyzed parallel and perpendicular to the nanowire axis. The nanowire affixed on the xy translation stage was scanned with a step size of 50 nm (accuracy of 1.5 nm). At each step, the scattered Raman spectrum was recorded at different combinations of incident polarization and analyzer orientation relative to a fixed nanowire azimuth. A single Lorentz function was fitted to the Raman spectrum obtained using linear polarization, $z(x,x)\overline{z}$ setting (LO-active), to determine the peak frequency of LO phonons. On the other hand, a double Lorentz fit function was applied for $z(x,y)\overline{z}$ setting (TO-active) to decompose and determine the peak frequency of TO phonons. As demonstrated below, this is justified by the coexistence of both LO and TO phonons in the obtained spectrum. It should be stressed that during double Lorentzian fitting, the LO peak position was fixed and assumed equal to the value obtained from the single Lorentzian fit of $z(x,x)\overline{z}$ setting. This was done at each position in the nanowire simply because the LO phonon peak position varies along the nanowire due to the nonuniform distribution of strain. Likewise, single and double Lorentzian fittings were applied for the incident azimuthal and radial polarization, respectively. This is because azimuthal polarization detects mostly LO phonon while radial polarization excites and detects both LO and TO phonons. In the double Lorentzian fit of

radial polarization, the LO peak value was fixed and takes the value obtained from the single Lorentzian fit of the azimuthal polarization. An exposure time of 120 and 30 s at 145 μW power was used for TO-active and LO-active condition, respectively. At this experimental condition, we made sure that heating due to laser energy is negligible by systemically analyzing the measured signals as a function of the laser power in the range of 31−316 μW.[35] It is also worth mentioning that the dimensions of strained Si nanowires (thickness = 15 nm and width = 30 nm) are large enough to prevent phonon confinement effects.[35,36]

The scattering efficiency, I, depends on the polarization vector of both the incident (e_i) and the scattered (e_s) light, and is generally expressed as[37]

$$ I \propto \sum_j |\mathbf{e}_s^T \mathbf{R}_j \mathbf{e}_i|^2 \tag{1} $$

where $\mathbf{R}_j$ is the Raman polarizability tensor for j^{th} active phonon mode and $\mathbf{e}_i$ and $\mathbf{e}_s$ are the incident and scattered electric field unit vectors, respectively. The superscript T denotes transpose of the scattered electric field vector. The Raman tensor for Si in the absence of stress is derived by Loudon[37] and expressed in crystal coordinate system $X = [100]$, $Y = [010]$ and $Z = [001]$. They are given by

$$ R_X = \begin{pmatrix} 0 & 0 & 0 \\ 0 & 0 & d \\ 0 & d & 0 \end{pmatrix}, \quad R_Y = \begin{pmatrix} 0 & 0 & d \\ 0 & 0 & 0 \\ d & 0 & 0 \end{pmatrix}, $$

$$ R_Z = \begin{pmatrix} 0 & d & 0 \\ d & 0 & 0 \\ 0 & 0 & 0 \end{pmatrix} \tag{2} $$

where d is a constant that is dependent on the Raman polarizability of the sample. For backscattering from a (001) surface, R_X and R_Y are the Raman tensor by the TO_1 and TO_2, respectively, whereas R_Z corresponds to LO phonons. In order to accurately obtain the contributions from LO and TO, we quantitatively compare the intensities of LO and TO phonons at different incident polarizations (linear, radial, and azimuthal) using a high NA lens. Since the edges of the nanowire are aligned along [110] direction, the Si Raman tensor in the crystal axes (XYZ) needs to be transformed in the sample coordinate (xyz) axes using tensor rotation. The Raman tensor in the sample coordinate axes is[38]

$$ R'_x = \frac{1}{\sqrt{2}} \begin{pmatrix} 0 & 0 & d \\ 0 & 0 & d \\ d & d & 0 \end{pmatrix}, \quad R'_y = \frac{1}{\sqrt{2}} \begin{pmatrix} 0 & 0 & d \\ 0 & 0 & -d \\ d & -d & 0 \end{pmatrix}, $$

$$ R'_z = \begin{pmatrix} d & 0 & 0 \\ 0 & -d & 0 \\ 0 & 0 & 0 \end{pmatrix} \tag{3} $$

In the typical backscattering configuration of most microscopes, the z-axis is taken as the laser beam propagation direction, while the analyzer, e_s, polarization direction takes either x- or y-axis. In this work, we utilized a high NA lens to take advantage of the higher z-component of light at the focus. On the basis of the Raman polarization selection rules,[28,38] this z-polarized light excites the TO phonons. However, as we increase the NA of the lens, the depolarized (y-component) light at the focus also

increases and becomes comparable to the z-component for linearly x-polarized incident light.[39] This contribution from depolarized light cannot be eliminated when scattered Raman is analyzed as in the case of polarized micro-Raman measurements, that is, $z(x, y)\bar{z}$. In order to describe the scattering process that involves illumination and collection by high NA lens, we cannot assume e_i to be constant across the focal volume. In the focus, the polarization of light has components along x, y, and z.[40] For instance, in the $z(x, y)\bar{z}$ setting, the excited LO phonon arising from the generated depolarized (y-polarized) field overlaps with the TO phonon resulting from the created longitudinal (z-polarized) field. To take into account the effects of the x, y, and z-components of the light on the intensity of detected Raman, numerical calculations aimed to determine the electric field intensity ($|e_i|^2$) distributions from a tightly focused lens were performed for 15 nm thick strained Si membrane. The resulting values are operated to the transformed Si Raman tensor to estimate the Raman intensities of LO and TO phonons. Another factor we need to examine is the change in the amplitude of the x- and y-polarized light during laser focusing into Si membrane, which has a very high refractive index comparable to bulk silicon ($n = 4.15 + 0.043i$ at 532 nm).[41] This change in the amplitude of the x- and y-polarized light can be easily taken into account by calculating the Fresnel equations in order to obtain the transmission and reflection coefficients of p- and s-polarized light at different media of known refractive index.[42] In this particular experiment, light propagates into a three-layer system consisting of oil (0th from oil-immersion objective lens), strained-Si (1st) and SiO_2 (2nd). These Fresnel coefficients were calculated by taking into account the multiple reflections at oil/strained Si and strained Si/SiO_2 interfaces. We neglect the contributions from the highly absorptive Ge-layer in the model because the polarized micro-Raman setup is confocal and that the multiple reflections from Ge-layer are assumed to be small due to the high refractive index of Ge. To model the effect of the high NA lens used for illumination on the Raman spectrum, we numerically calculated the ($|e_i|^2$) over the finite solid angle subtended by the objective. Hence, to integrate all the non-negligible effects discussed above on the intensity of the Raman mode, eq 1 can be replaced by

$$ I_i = I_0 \sum_i \int_0^{2\pi} \int_0^{\theta_{max}} \left| \left[R(\alpha, \beta, \gamma) \begin{pmatrix} E_{scaX}(\theta, \phi, \eta) \\ E_{scaY}(\theta, \phi, \eta) \\ E_{scaZ}(\theta, \phi, \eta) \end{pmatrix} \right]^T \right. $$
$$ \left. \times \left[R_i \cdot R(\alpha, \beta, \gamma) \begin{pmatrix} E_x \\ E_y \\ E_z \end{pmatrix} \right] \right|^2 \sin\theta \, d\theta \, d\phi \tag{4} $$

where, I_0 is the incident intensity, η is the angle setting of the analyzer with respect to the x-axis, and θ and ϕ are the polar and azimuthal angles. The explicit form of E_x, E_y, and E_z depends on whether radial, azimuthal, or linear incident polarization is used (see Supporting Information, Section A). $E_{sca}(\phi, \theta, \eta)$ is the scattered electric field defined from the objective transfer matrix that describes the radiation dipole collection efficiency of a high NA objective lens (See Supporting Information, Section A). R_i is the Raman tensor in the crystal coordinate (XYZ) system, which can be easily transformed into sample coordinate (xyz) system using the well-known Euler rotation matrix,[43] $R(\alpha, \beta, \gamma)$
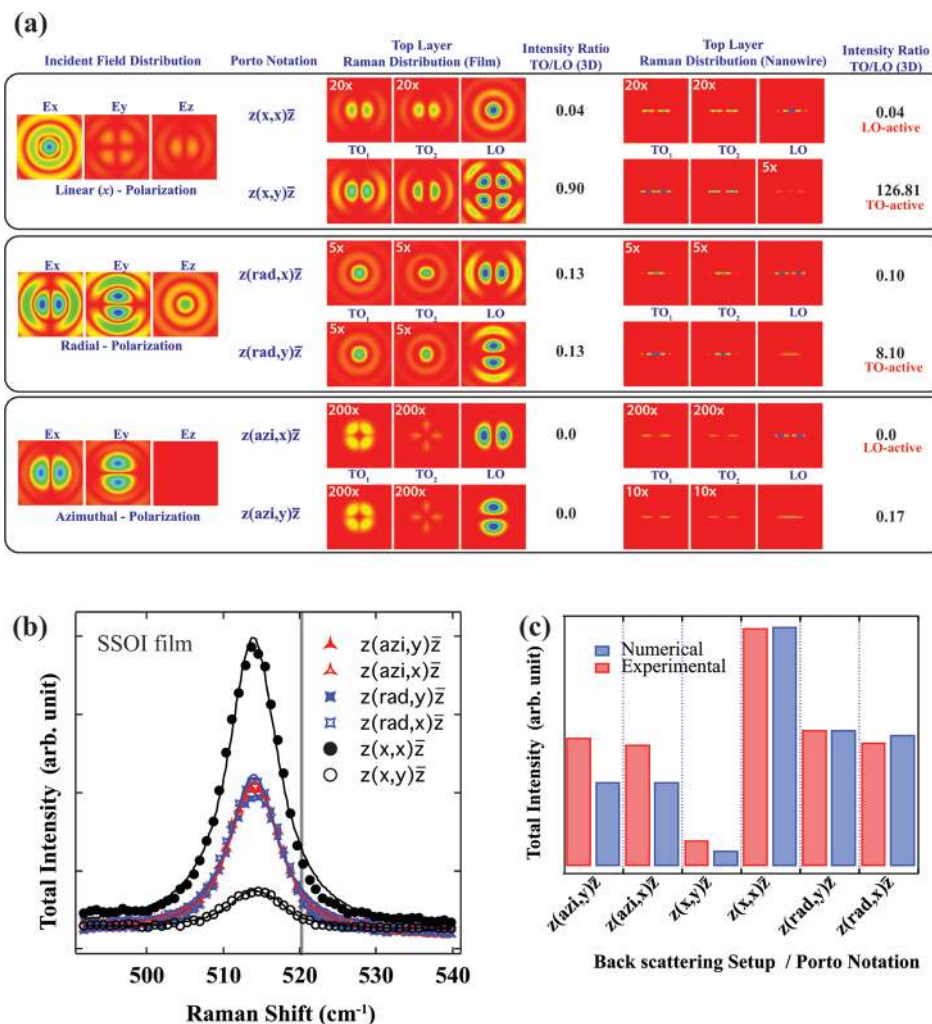
Figure 2. (a) Electric field distribution on the surface of the strained Si membrane and the corresponding calculated Raman intensities (normalized at each setting) using eq 4 at various analyzer and polarizer settings. Image size is $1 \times 1 \ \mu m^2$. For each setting, the TO/LO Raman intensities were calculated in three-dimensional (3D) and tabulated. Note: The observed maximum Raman intensity is found at the SiO$_2$ and strained Si interface. (b) Raman spectra measured from the strained membrane at different experimental configurations. (c) Comparison between numerical and experimental normalized total intensities obtained from panels a and b.

(see Supporting Information Section C). The integration over the solid angle, $\sin \theta \ d\theta d\phi$, is confined only to the collection cone for the scattered light. This scattered intensity is a complex function whose explicit form is determined by the Raman polarizability tensors. In the absence of stress, the three optical phonons of Si have the same frequency (degenerate).[28] However, in the presence of stress, these Raman modes lift their degeneracy. Therefore, aside from the changes in the intensity of the Raman mode, variations in the frequency of LO and TO phonons can be analyzed.

LO and TO phonons in UT-SSOI membrane. Figure 2a shows the numerically obtained $1 \times 1 \ \mu m^2$ electric field distributions at the surface of strained Si at different polarizations. These distributions were obtained for a 532 nm light source focused with a high NA ($1.0 \leq NA \leq 1.4$) oil lens (See Figure S2 in Supporting Information). The electric field distributions were normalized at each incident polarization for comparison. For linearly x-polarized light, it can be seen that the depolarized, y-, and normal, z-components, are nonzero with comparable amplitude. This suggests that for high NA illumination, the three Raman modes in eq 4 are excited. The excited

Raman intensity of the three Raman modes denoted by TO$_1$, TO$_2$, and LO can be determined by operating the field distribution with the Raman tensor of Si at different analyzer settings as indicated in Figure 2a. Similar to electric field distribution, the calculated excited Raman intensity for each analyzer setting was also normalized for the sake of clarity. The normalization is done relative to the maximum Raman intensity for each analyzer setting. In the case of Si nanomembrane (film), the Raman intensity is normalized to the maximum intensity of the excited LO signal for each analyzer setting. But in the case of nanowires, Raman intensity is normalized to maximum Raman intensity of either TO$_1$ or LO signal. From this we note that the normalized LO intensity in $z(x, x)\bar{z}$ is of the same contrast as the normalized LO in the $z(x, y)\bar{z}$ setting. The normalized TO intensity in the $z(x, x)\bar{z}$ setting have the same intensity as normalized TO in the $z(x, y)\bar{z}$ setting. Thus, the LO intensity is very strong compared to TO intensity even after scaling the value of TO to 20 times. When the analyzer is set parallel to y-axis ($\eta = 90$), TO and LO can be detected simply because the strong LO excited by x-polarized light is mostly blocked by the analyzer. In polarized

micro-Raman spectroscopy under backscattering geometry, the system setting described above is represented as $z(x, y)\bar{z}$ in Porto notation. Though both $z(x, x)\bar{z}$ and $z(x, y)\bar{z}$ settings contain LO and TO modes, the TO/LO ratio difference between settings is significant. In the case of $z(x, y)\bar{z}$, the TO/LO ratio is $\sim$0.90. On the other hand, for $z(x, x)\bar{z}$, TO/LO ratio is $\sim$0.04. Owing to this, we define the $z(x, y)\bar{z}$ setting as TO-active and the $z(x, x)\bar{z}$ as LO-active. The TO/LO ratio is calculated by integrating the intensity in three dimensions over the 15 nm thick UT-SSOI membrane and over the diffraction-limited focus spot, which is defined by 1.22λ/NA ($\sim$464 nm). For the radially polarized light, we can generate relatively higher z-components, $\sim$2$\times$, of the light compared to linear polarization. However, both x- and y-components have the same light intensity unlike in linear polarization where the depolarized light is weak and somewhat comparable to z-components. Nevertheless, radially polarized light can also be suitable for TO characterization because TO spatial resolution is approximately twice better as compared to linear polarization. The Raman intensity distribution of radially polarized light is tightly focused and locally observed at the center as opposed to the two intense split feature of the field distribution in the linear polarization. For azimuthal polarization, mostly LO mode is detectable because the z-components of the electric field are zero. Thus we define azimuthal polarization as LO-active and radial polarization as TO-active. The difference in the intensity of TO_1 and TO_2 in Figure 2a can be easily understood from polarization selection rules.[28,37] In TO_2, the generated Raman arising from the transverse electric fields cancels each other because of the presence of negative sign in the Raman tensor, R_y' (See eq 3). In the case of TO_1, the Raman signals excited from the transverse fields add up. Figure 2b shows some variations in the total Raman intensity at different experimental configurations. The total intensity (area under each Raman spectrum) was determined and compared with numerically calculated intensity in Figure 2a. Figure 2b shows the Raman spectra from the strained membrane at various incident and scattered polarizations. The measured Si—Si Raman peak was found to be centered at $\sim$514.3 cm^{-1}, about $\sim$6.2 cm^{-1} below its unstrained Si—Si peak (gray vertical line) position, $\sim$520.5 cm^{-1} at room temperature.[44] The biaxial strain is estimated using[21]

$$\omega_{\varepsilon-\mathrm{Si}} = \omega_{\mathrm{Si}} + \frac{1}{\omega_{\mathrm{Si}}}\left(q + \frac{S_{12}}{S_{11} + S_{12}}p\right)\frac{(\varepsilon_{xx} + \varepsilon_{yy})}{2} \quad (5)$$

where ε_{xx} and ε_{yy} are the two in-plane strain components, $\omega_{\varepsilon-\mathrm{Si}}$ and ω_{Si} are the Raman frequency shifts (in cm^{-1}) of strained and unstrained Si, respectively. The $S_{11} = 7.68$ and $S_{12} = -2.14$ (in GPa) are the elastic compliance tensor elements, while $p = -1.85 \times \omega_{\mathrm{Si}}^2$ and $q = -2.31 \times \omega_{\mathrm{Si}}^2$ are the phonon deformation potentials for bulk Si.[45,46] The sensitivity and reliability of strain analysis based on eq 5 were confirmed using strained nanomemebranes with different strain levels and TEM-based methods. The corresponding biaxial tensile strain of $\varepsilon_{xx} = \varepsilon_{yy} = 0.75\%$ was estimated for the membrane. Figure 2c shows the comparison of the numerical and experimental results. Good agreement between the two sets of data is observed.

LO and TO Phonon Profiles in Strained Si Nanowire. When characterizing strain in nanoscale devices such as strained nanowires, it is very important to know the location of the peak position or high intensity areas of the E_x, E_y, and E_z light components relative to the nanostructure. This is because the detected Raman can either be LO or TO or a combination of both modes depending on the location of the nanowire relative to the peak position of the field at the focus. From the calculations described in Figure 2a, the best setting to obtain LO and TO optical phonon at the same position on the strained Si nanowire is to locate the nanowire at the center of the focus and first obtain LO peak position using $z(x, x)\bar{z}$ and then switch to radial polarization by inserting the Z-pol to obtain the peak position of TO using $z(\mathrm{rad}, y)\bar{z}$ setting. This is because the intense part of Raman intensity distributions for LO and TO are colocated at the center of the focus for both the $z(x, x)\bar{z}$ and $z(\mathrm{rad}, y)\bar{z}$ setting as indicated in Figure 2a.

Figure 2a shows the calculated Raman distribution from TO-active, $z(x, y)\bar{z}$ and $z(\mathrm{rad}, y)\bar{z}$ configuration for strained Si nanowire with lateral dimensions of 30 nm and 1 μm and a thickness of 15 nm. We can see that TO/LO ratio increases significantly for the nanowire under $z(x, y)\bar{z}$ and $z(\mathrm{rad}, y)\bar{z}$ setting and reaches 126.81 and 8.10, respectively. This calculated TO/LO intensity ratio is one to 2 orders of magnitude higher compared to the calculated ratio for the strained membrane. It is important to mention that the TO/LO ratio changes depending on the width of the nanowire. Another interesting observation is that the characterized area (strength and location of Raman peak intensities) along the nanowire between $z(x, y)\bar{z}$ and $z(\mathrm{rad}, y)\bar{z}$ setting is different. The sensitivity of TO detection under linear polarization is higher than radial polarization based on the TO/LO ratio. However, the strength of the TO Raman signal in radial polarization is higher than linear polarization at a fixed laser power. Hence, radial polarization is advantageous compared to linear polarization when low power is needed for TO characterization in strained nanowire. This is because nanowire heats up easily compared to the strained membrane.

Figures 3a,b shows the measured Raman spectra at the center of a single UT-SSOI nanowire using $z(x, y)\bar{z}$ and $z(\mathrm{rad}, y)\bar{z}$ settings, respectively. For comparison, the measured Raman from LO-active, $z(x, y)\bar{z}$ and $z(\mathrm{azi}, x)\bar{z}$, configurations were plotted. We can clearly see that the TO-active is broader than the LO-active condition for both radial and linear incident polarizations (Note that the spectral accuracy for this analysis is $\sim$0.02 cm^{-1}). This is because the TO-active condition consists of contributions from both LO and TO phonons. Note that the data presented is taken at the same laser power and that is not deconvoluted with system spectral resolution and laser line width. The broadening of the Raman width can be interpreted as strain-dependent overlap of the nondegenerate three-phonon modes. The Si—Si LO mode peak position is centered at $\sim$516.7 cm^{-1}, which is 2.4 cm^{-1} above the value in the initial membrane ($\sim$514.3 cm^{-1}) in Figure 2b (See also Figure S4 in Supporting Information). This strain relaxation is result of formation of free surfaces during patterning (RIE process). The obtained LO peak parameters in the $z(x, x)\bar{z}$ setting were utilized to fit the LO peak position in the double Lorentzian fitting of the measured spectra from $z(x, y)\bar{z}$ configuration to determine the peak of Si—Si TO phonons. We found that the Si—Si TO peak position located at $\sim$517.7 cm^{-1} ($\sim$1.0 cm^{-1} blueshifted with respect to LO phonon) corresponding to lower strain. The TO/LO intensity ratio, obtained by integrating the Raman spectrum, was found to be 1.5 and 0.9 for $z(x, y)\bar{z}$ and $z(\mathrm{rad}, y)\bar{z}$ settings, respectively. This measured TO/LO intensity ratio agrees qualitatively with the calculation in Figure 2a where the TO/LO ratio is higher in $z(x, y)\bar{z}$ than $z(\mathrm{rad}, y)\bar{z}$ settings. The variation in the magnitude of the measured TO/LO in Figure 3a,b to that of the calculated TO/LO in Figure 2a can be due to the alignment deviations, which is found to be very sensitive to the position and actual diameter of the UT-SSOI relative to the
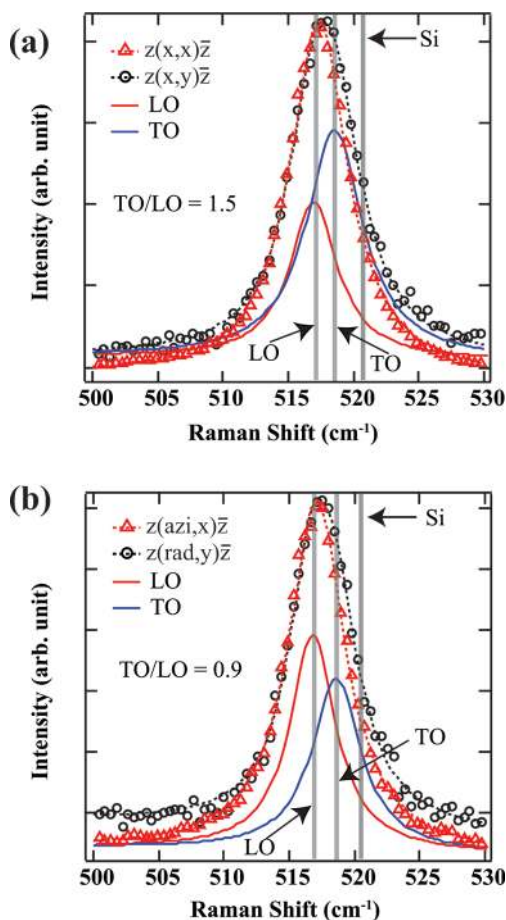
Figure 3. Raman spectra measured at the center of the nanowire for (a) $z(x, y)\bar{z}$ and (b) $z(\text{rad}, y)\bar{z}$ TO-active settings. For comparison, recorded Raman spectra from LO-active, $z(x, x)\bar{z}$ and $z(\text{azi}, x)\bar{z}$, were also plotted. The solid red (LO) and blue (TO) lines are the result of the double Lorentzian fit under the TO-active setting. The dashed red (LO) line is the fit of Raman peak under LO-active setting. The gray vertical lines denote Raman peak positions for bulk Si, LO, and TO phonons of strained silicon.

Figure 4. Profiles of TO peak (primary y-axis) and the LO peak (secondary y-axis) positions across the nanowire under (a) $z(x, y)\bar{z}$ and (b) $z(\text{rad}, y)\bar{z}$ TO-active settings. (c) Profile of the stress-ratio between singlet and doublet phonons along the nanowire. The x-position is parallel to the [110] direction. Horizontal line is the theoretical value for stress ratio using eqs 6 and 7. The gray bar in the plot presents the strained nanowire.

center of the focus. Moreover, the variation can be partly attributed to the edges of the patterned structures, which are aligned along the [110] direction. This is because for backscattering from (110) surface, either the LO or the TO can be excited and detected based on selection rules.[38]

Figure 4a shows the profiles of Si−Si peak for TO (primary y-axis) and LO (secondary y-axis) along the nanowire at a 50 nm step. The gray bar in the plot presents the strained nanowire and can be used to correlate the measured Raman and the position on the nanowire where data is obtained. The plotted data are the average from two scans across the length of the same nanowire under the same experimental conditions. We observed that both LO and TO relaxations become more pronounced away from the center of the nanowire. The difference in the behavior between linear and radial incident polarizations can be due to both TO/LO sensitivity and spatial resolution associated with them (see Figures 2a and 3a). For the linear setting, both TO and LO profiles display a plateau at $300 \leq L \leq 700$ nm, which means that the stress is nearly constant in this region. The stress then drastically decreases toward the edges of the nanowire. For radial setting, both TO and LO decrease monotonically and somewhat follows a parabolic behavior. The slight
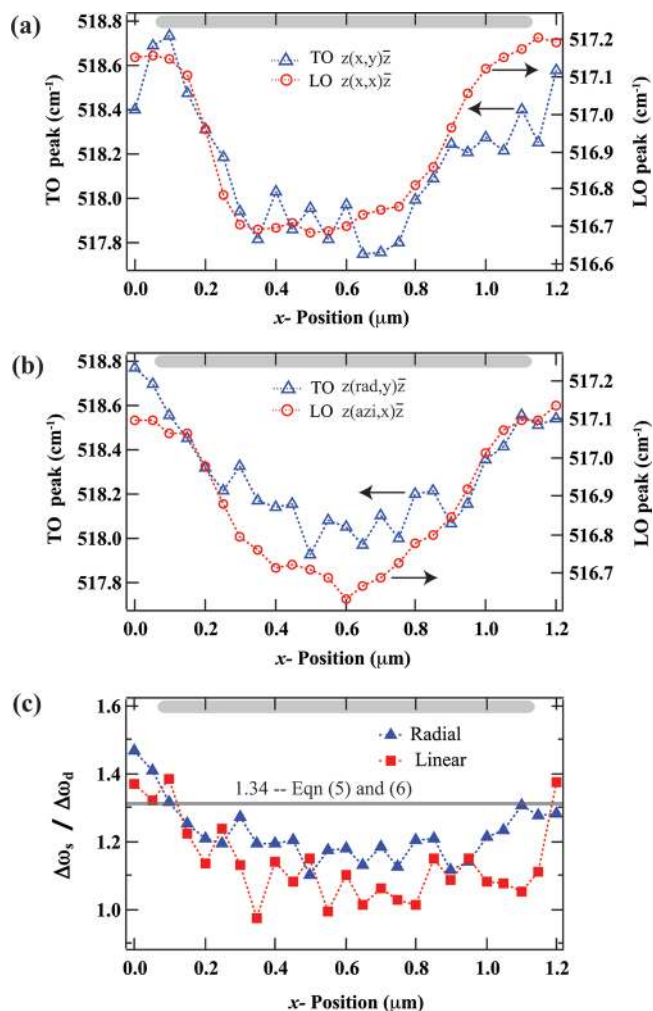
difference in the TO profile between the two polarizations could be due the presence of two intense peaks in linear polarization versus single intense peak in radial polarization.

For a strained nanowire, the actual stress along the σ_{xx} and the σ_{yy} are generally not equal and vary with the width and length of the nanowire due to the edge-induced relaxation.[46] Note that the strain remains biaxial but not bi-isotropic as it is in the initial strained membrane. The stress-induced Raman phonon shifts can be obtained by solving the well-known secular equation.[38] In the case of (001) in-plane biaxial tensile stress and with the assumption that $\sigma_{xx} = \sigma_{yy} = \sigma$ ($xx \parallel [110]$, $yy \parallel [110]$) and $\sigma_{zz} = 0$ ($zz \parallel [001]$), the stress-induced Raman shift for doublet ($\Delta\omega_d$, TO phonons) and singlet ($\Delta\omega_s$, LO phonons) are

$$\Delta\omega_d = \frac{[p(\mathbf{S}_{11} + \mathbf{S}_{12}) + q(\mathbf{S}_{11} + 3\mathbf{S}_{12})]\sigma}{2\omega_0} = -3.42 \times \sigma \qquad (6)$$

$$\Delta\omega_s = \frac{[p\mathbf{S}_{12} + q(\mathbf{S}_{11} + \mathbf{S}_{12})]\sigma}{\omega_0} = -4.60 \times \sigma \qquad (7)$$
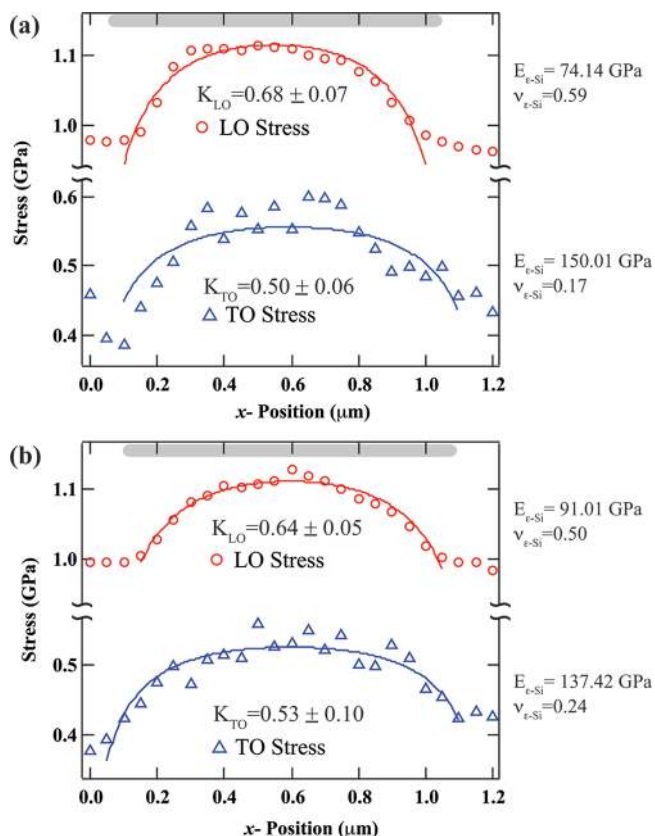
Figure 5. Profiles of LO and TO stress along the wire using (a) linear and (b) radial polarizations. The TO and LO stress were calculated from eqs 6 and 7, respectively. The x-position is parallel to the [110] direction. The solid curves are obtained by fitting eq 8. K is the relative rigidity of the nanowire, which is a function of Young's modulus and Poisson ratio.

where $\Delta\omega_d = \omega_{\varepsilon-Si} - \omega_0$ and $\Delta\omega_s = \omega_{\varepsilon-Si} - \omega_0$ are expressed in the Raman frequency in each mode in the presence $(\omega_{\varepsilon-Si})$ and the absence (ω_0) of stress. Using the phonon deformation potential and the compliance tensor element values, listed above (see eq 5 and refs 45 and 46), the theoretical stress ratio $(\Delta\omega_s/\Delta\omega_d)$ is ~1.34. Figure 4c shows the variations in the experimentally obtained stress ratio $(\Delta\omega_s/\Delta\omega_d)$ along the nanowire for linear and radial polarizations. We can observe that the stress ratio at the edges of the nanowire approaches the theoretical value (gray horizontal line) of 1.34. However, it starts to deviate away from the theoretical value as we approach the center of the nanowire. The $\Delta\omega_s/\Delta\omega_d$ value at regions far from the edges is lower relative to the theoretical value. These observations indicate that far from the edges the strain becomes partially uniaxial ($\sigma_{xx} \neq \sigma_{yy}$ with $\sigma_{xx} \gg \sigma_{yy}$ as the relaxation is more pronounced along the shortest dimension) and it remains biaxial ($\sigma_{xx} = \sigma_{yy}$) near the edges. The fact that the most of the obtained stress ratio along the nanowire are lower than the theoretical value (using bulk parameters) may also indicate that further optimization of the deformation potentials is required for nanowires.

We have seen the relaxation of stress in the nanowire relative to the initial stress in the membrane. This TO and LO elastic stress relaxation, due to atomic displacement at patterning-induced free surfaces and edges, can be calculated using eqs 6 and 7. Figure 5a,b shows the calculated stress for LO and TO at different positions in the strained nanowire. It is

noticeable that the edges of the nanowire are more relaxed compared to the center. This behavior agrees with three-dimensional finite element simulations of strain distribution in patterned nanowires (see Figure S5 in Supporting Information). To describe this evolution as well as the associated mechanical properties of the nanowire, we combine Hu's model[47] of stress relaxation and the analysis done by Fischer et al.[48] to fit the stress behavior shown in Figure 5. The stress distribution can be fitted using the equation below

$$\sigma(x) = A\left(1 - \exp\left[-\sqrt{\frac{2Kx}{d\tau}}\right] - \exp\left[-\sqrt{\frac{2K(L-x)}{d\tau}}\right]\right)$$

$$K = \frac{E_{SiO_2}(1-v_{\varepsilon Si}^2)}{E_{\varepsilon Si}(1-v_{SiO_2}^2)} \quad \text{and} \quad (S_{11} + S_{12}) = \frac{(1-v_{\varepsilon Si}^2)}{E_{\varepsilon Si}} \tag{8}$$

where A is the proportionality constant which takes the maximum stress at the center and L is the length of the nanowire. The stress relaxation is dependent on the ratio of the thickness of the strained nanowire ($d \approx 15$ nm) and the relative rigidity K between the SiO_2 substrate and strained nanowire. The relative rigidity defined in eq 8 is a function of material mechanical property, where E and v denotes the Young's modulus and the Poisson ratio, respectively. Using the eq 8, the best-fit value for K is indicated in Figure 5 for both (a) linear and (b) radial polarizations. Both polarizations show that K for LO is greater than the K for TO stress relaxation. This suggests that relative rigidity is different for in-plane (LO) and out-of-plane (TO) directions. The difference in the obtained K between linear and radial polarizations can be due to sensitivity and spatial resolution of the measurements. On the basis of this observation, we can infer that the Young's modulus of the strained nanowire is anisotropic. The behavior and distribution of the stress also tells us about the mechanical material property of the strained nanowire. For the biaxial plane stress conditions typically associated with thin films, longitudinal stress and strain from (100) plane are related by $E/(1 - v)$ and the generalized expression for this composite elastic constant is a function of compliance tensor element. Knowing this direct relation between longitudinal stress and strain from eq 8, we can readily calculate $E_{\varepsilon Si}$ and $v_{\varepsilon Si}$ for strained Si nanowire from the relative rigidity fitted K value and using the material property of thin SiO_2 ($E_{SiO_2} = 75$ GPa and $v_{\varepsilon Si} = 0.17$) available from literature.[49] We note that the estimated out-of-plane elastic modulus (~140 GPa) is consistent with the atomistic calculations of elastic modulus of strained Si(001).[50] On the other hand, the in-plane value of the nanowire elastic modulus is relatively smaller (~80 GPa), but it remains comparable to the radial elastic modulus of Si(112) nanowires under compressive strain.[51] Though we made assumptions on the actual mechanical property of handle SiO_2 substrate, the method to determine the nanoscale mechanical characteristics of strained Si is nondestructive and could well be suited for other nanomaterials.

In summary, we have demonstrated a method to map the "forbidden" TO phonon mode in single ultrathin tensile strained Si nanowires with sufficient sensitivity and spatial resolution at different incident polarizations using high NA polarized micro-Raman spectroscopy. The introduction of a Ge intermediate layer improves the sensitivity by circumventing the issues associated with strong substrate background arising from the underlying substrate. We found that, unlike planar systems, the sensitivity to TO phonons is strong in nanowires. Detailed

evolutions of TO and LO phonons and their profiles in single nanowires were obtained using linearly and radially polarized light. The obtained profiles of each phonon display a qualitatively identical behavior, whereas a systematic blueshift is observed for TO phonon with respect to LO phonon indicative of the anisotropic relaxation of strain. This free surface-induced strain redistribution provides a wealth of opportunities to engineer locally the strain in Si nanowire-based devices.

■ ASSOCIATED CONTENT

S **Supporting Information.** Additional information. This material is available free of charge via the Internet at http://pubs.acs.org.

■ AUTHOR INFORMATION

Corresponding Author
*E-mail: (N.H.) hayazawa@riken.jp; (O.M.) moutanab@mpi-halle.mpg.de.

■ ACKNOWLEDGMENT

■ REFERENCES

(1) Chu, M.; Sun, Y.; Aghoram, U.; Thompson, S. E. *Annu. Rev. Mater. Res.* **2009**, *39*, 203.
(2) Celler, C. K.; Cristoloveanu, S. *J. Appl. Phys.* **2003**, *93*, 4955.
(3) Lauhon, L. J.; Gudiksen, M. S.; Wang, D.; Lieber, C. M. *Nature* **2002**, *420*, 57.
(4) Ieong, M.; Doris, B.; Kedzierski, J.; Rim, K.; Yang, M. *Science* **2004**, *306*, 2057.
(5) Jacobsen, R. S.; Andersen, K. N.; Borel, P. I.; Fage-Pederson, J.; Frandsen, L. H.; Hansen, O.; Kristensen, M.; Lavrinenko, A. V.; Moulin, G.; Ou, H.; Peucheret, C.; Zsigri, B.; Bjarklev, A. *Nature* **2006**, *441*, 199.
(6) Lyons, D. M.; Ryan, K. M.; Morris, M. A.; Holmes, J. D. *Nano Lett.* **2002**, *2*, 811.
(7) Hong, K.-H.; Kim, J.; Lee, S.-H.; Shin, J. K. *Nano Lett.* **2008**, *8*, 1335.
(8) Wu, Z.; Neaton, J. B.; Grossman, J. C. *Nano Lett.* **2009**, *9*, 2418.
(9) Kanai, Y.; Wu, Z.; Grossman, J. C. *J. Mater. Chem.* **2010**, *20*, 1053.
(10) Nduwimana, A.; Wang, X.-Q. *J. Phys. Chem. C* **2010**, *114*, 9702–9705.
(11) Hashemi, P.; Gomez, L.; Hoyt, J. L. *IEEE Electron Device Lett.* **2009**, *30* (4), 401.
(12) Goldthorpe, I. A.; Marshall, A. F.; McIntyre, P. C. *Nano Lett.* **2009**, *9* (11), 3715.
(13) Eneman, S.; Verheyen, P.; Rooyackers, R.; Nouri, F.; Washington, L.; Degraeve, R.; Kaczer, B.; Moroz, V.; De Keersgieter, A.; Schreutelkamp, R.; Kawaguchi, M.; Kim, Y.; Samoilov, A.; Smith, L.; Absil, P. P.; De Meyer, K.; Jurczak, M.; Biesemans, S. *VLSI Technol.* **2005**, 22.
(14) Moutanabbir, O.; Reiche, M.; Hähnel, A.; Erfurth, W.; Gösele, U.; Motohashi, M.; Tarun, A.; Hayazawa, N.; Kawata, S. *Appl. Phys. Lett.* **2010**, *96*, 233105.
(15) Tarun, A.; Hayazawa, N.; Kawata, S. *Anal. Bioanal. Chem.* **2009**, *394*, 1775–1785.
(16) Hytch, M.; Houdellier, F.; Hue, F.; Snoeck, E. *Nature* **2008**, *453*, 1086.
(17) Béché, A.; Rouviére, J. L.; Clément, L.; Hartmann, J. M. *Appl. Phys. Lett.* **2009**, *95*, 123114.
(18) Robinson, I.; Harder, R. *Nat. Mater.* **2009**, *8*, 291.
(19) Baudot, S.; Andrieu, F.; Rieutord, F.; Eymery, J. *J. Appl. Phys.* **2009**, *105*, 114302.
(20) Motohashi, M.; Hayazawa, N.; Tarun, A.; Kawata, S. *J. Appl. Phys.* **2008**, *103*, 034309.
(21) Moutanabbir, O.; Reiche, M.; Hähnel, A.; Erfurth, W.; Gösele, U.; Motohashi, M.; Tarun, A.; Hayazawa, N.; Kawata, S. *Nanotechnology* **2010**, *21*, 134013.
(22) Moutanabbir, O.; Reiche, M.; Hähnel, A.; Oehme, M.; Kasper, E. *Appl. Phys. Lett.* **2010**, *97*, 053105.
(23) Parker, J. H., Jr; Feldman, D. W.; Ashkin, M. *Phys. Rev.* **1967**, *155*, 712.
(24) Mayuzumi, S.; et al. *IEDM Tech. Dig.* **2007**, 293.
(25) Brunner, K.; Abstreiter, G.; Kolbesen, B. O.; Meul, H. W. *Appl. Surf. Sci.* **1989**, *39*, 116.
(26) Loechelt, G. H.; Cave, N. G.; Menéndez, J. *J. Appl. Phys.* **1999**, *86*, 6164.
(27) Ossikovski, R.; Nguyen, Q.; Piccardi, G.; Schreiber, J. *J. Appl. Phys.* **2008**, *103*, 093525.
(28) Anastassakis, E. *J. Appl. Phys.* **1997**, *82*, 1582.
(29) Bonera, E.; Fanciulli, M.; Batchelder, D. N. *J. Appl. Phys.* **2003**, *94*, 2729.
(30) Ossikovski, R.; Nguyen, Q.; Piccardi, G.; Schreiber, J.; Morin, P. *J. Raman Spectrosc.* **2008**, *39*, 661.
(31) Kosemura, D.; Ogura, A. *Appl. Phys. Lett.* **2010**, *96*, 212106.
(32) Poborchii, V.; Tada, T.; Kanayama, T. *Appl. Phys. Lett.* **2010**, *97*, 041051.
(33) Tarun, A.; Hayazawa, N.; Motohashi, M.; Kawata, S. *Rev. Sci. Instrum.* **2008**, *79*, 013706.
(34) Hayazawa, N.; Saito, Y.; Kawata, S. *Appl. Phys. Lett.* **2004**, *85*, 6239.
(35) Adu, K. W.; Gutiérrez, H. R.; Kim, U. J.; Eklund, P. C. *Phys. Rev. B* **2006**, *73*, 155333.
(36) Roodenko, K.; Goldthorpe, I. A.; McIntyre, P. C.; Chaba, Y. J. *Phys. Rev. B* **2010**, *82*, 115210.
(37) Loudon, R. *Adv. Phys.* **1964**, *13*, 423–80.
(38) De Wolf, I. *Semicond. Sci. Technol.* **1996**, *11*, 139.
(39) Cooper, I. J.; Roy, M.; Sheppard, C. J. R. *Opt. Express* **2005**, *13*, 1066–71.
(40) Turell, G. *Raman Microscopy: Developments and its Applications*; Turell, G., Corset, J., Eds.; Academic: London, 1996.
(41) *Handbook of optical Constants of Solids*; Palik, E. D., Ed.; Academic Press: Boston, 1985.
(42) *Principles of Optics*; Born, M., Wolf, E., Eds.; Macmillan: New York, 1964.
(43) Hopkins, J. B.; Farrow, L. A. *J. Appl. Phys.* **1986**, *59*, 1103.
(44) Richter, H.; Wang, Z. P.; Ley, L. *Solid State Commun.* **1981**, *39*, 625.
(45) Anastassakis, E.; Cantanero, A.; Cardona, M. *Phys. Rev. B* **1990**, *41*, 7529.
(46) Jain, S. C.; Dietrich, B.; Richter, H.; Atkinson, A.; Harker, A. H. *Phys. Rev. B* **1995**, *52*, 6247.
(47) Hu, S. M. *J. Appl. Phys.* **1991**, *70*, R53.
(48) Fischer, A.; Richter, H. *J. Appl. Phys.* **1993**, *75*, 657.
(49) Kim, M. T. *Thin Solid Films* **1996**, *283*, 12–16.
(50) Zhu, R.; Pan, E.; Chung, P.; Cai, X.; Liew, K. M.; Buldum, A. *Semicond. Sci. Technol.* **2006**, *21*, 906.
(51) Stan, G.; Krylyuk, S; Davydov, A. V; Cook, R. F. *Nano Lett.* **2010**, *10*, 2031.